ORIGINAL RESEARCH **Open access**

Low-Cost UAV Photogrammetric Workflow for Tree Height Estimation in Heterogeneous Vegetation

Pieter Botha[1*], Anel Van Wyk[1], Johan Marais[2], Thabo Nkosi[3]

Abstract

In precision agriculture (PA), geomatic data collection using UAV (unmanned aerial vehicle) systems enables dimensional assessment of trees. This work investigates the application of affordable UAV photogrammetry for estimating tree height, forming part of a project focused on the phytoremediation of polluted soils. Two test sites with contrasting average tree stature (5 m; 0.7 m) were selected to evaluate the methodology, including under difficult conditions. Three data acquisition flights were undertaken in an olive grove (Area 1) at different altitudes above ground (30 m, 40 m, and 50 m), and one UAV overflight is available for Area 2 (42 m altitude), which contains three vegetation types: oleander, lentisk, and poplar. The processing sequence encompasses the generation of UAV point clouds using the SfM (structure from motion) technique, the creation of digital surface models (DSMs), the removal of vegetation returns, and a GIS-supported analysis to derive canopy height models (CHMs) for extracting heights via a local maxima algorithm. Heights obtained from the UAV are checked against ground-truth measurements, yielding encouraging results in Area 1 and corroborating the method's viability for tree height retrieval. In contrast, deployment in Area 2 (which comprises shorter saplings) is more challenging.

Keywords UAV, Photogrammetry, Precision Agriculture (PA), Local maxima algorithm, SfM, QGIS

*Correspondence:
Pieter Botha
pieter.botha@sun.ac.za
[1] Department of AI for Rooibos and Citrus Orchard Pest Management, Faculty of Agriculture, Stellenbosch University, Stellenbosch, South Africa
[2] Department of Smart Weather Station Network Analytics, Faculty of Agriculture, University of Pretoria, Pretoria, South Africa
[3] Department of Machine Learning for Wildfire Risk Reduction, Faculty of Agriculture, University of Cape Town, Cape Town, South Africa

Introduction

Precision agriculture (PA) can be understood as a site-specific crop management strategy grounded in the observation, measurement, and reaction to a suite of quantitative and qualitative variables that influence agricultural output [1]. The foundational step in the PA framework is capturing and assembling data from diverse sensors, such as optical, multispectral, and geophysical instruments, to develop a comprehensive characterization of vegetation and track a crop's status [2]. Accordingly, PA typically incorporates a broad spectrum of methods and technologies that require appropriate integration to advance progressively more sustainable farming stewardship [3, 4]. In this respect, merging datasets from heterogeneous sources depends on the diligent handling of coordinate reference frameworks, usually managed via geographic information systems (GISs), which serve as highly appropriate platforms for cross-disciplinary investigations [5, 6]. Among available technologies, geophysics and geomatics approaches constitute essential decision-support instruments for PA implementations, delivering critical intelligence for crop preservation and oversight [7].

This is an open access article distributed under the terms of the Creative Commons Attribution-NonCommercial-ShareAlike 4.0 International License (CC BY-NC-SA 4.0), which permits non-commercial use, distribution, reproduction, and adaptation in any medium or format, provided that appropriate credit is given to the original author(s) and source, a link to the license is provided, and any changes made are indicated. Adapted material must be distributed under the same license.

© 2024 The Author(s). | Published by Agro Intelligence Research Press

In particular, geophysical assessments assess the chemical properties of plants and the uppermost subsurface layers, employing purpose-built devices such as ground-penetrating radar systems [8, 9]. In a complementary fashion, geomatics techniques enable the derivation of quantitative metrics describing vegetation, including height, crown width, and volumetric extent. The deployment of global navigation satellite systems (GNSSs) within agriculture dates back to the 1990s, coinciding with the advent of farm machinery equipped with GNSS receivers. Nonetheless, employing GNSS tools to gather field observations cannot ensure dense data coverage without incurring exceedingly laborious and costly survey campaigns [10]. As a result, within this framework, they are routinely employed as auxiliary inputs to other methodologies. By the early 2000s, uncrewed aerial vehicles had become transformative components of precision agriculture, serving as highly practical platforms for deploying a range of sensors (e.g., LiDAR, multispectral, and optical cameras). The primary strengths of unmanned aerial vehicles (UAVs) indeed lie in their rapid operational tempo and lower costs compared with competing geomatic approaches [11, 12].

A multitude of studies have examined the use of UAV-acquired remote sensing data for silvicultural or agricultural purposes, largely relying on LiDAR (light detection and ranging) datasets or multispectral imagery [9, 13-20]. Additionally, the bulk of these implementations are situated in woodland environments, where stands of tall, closely spaced trees occur, and the main emphasis is on crown detection and species or health classification [14, 15, 17, 21-24]. In contrast, newer inquiries have been conducted across zones with lower-growing vegetation, drawing on either photogrammetric or LiDAR sources [16, 25-30]. Notably, the extraction of tree heights from UAV-captured optical imagery has been addressed by multiple investigators, with diverse specific features of the surveyed plants, yielding broadly promising outcomes [14, 21, 23, 31, 32]. In LiDAR point clouds, photogrammetric outputs are generally understood to exhibit higher noise levels and lower fidelity, as they capture only the outer canopy envelope without penetrating to the terrain below [14]. Conversely, data characterizing bare earth can be recovered from LiDAR surveys by exploiting multiple-return pulses that can penetrate gaps in the foliage [33, 34]. This capability consistently improves the accuracy of ground surface representation, which is fundamental for a faithful three-dimensional reconstruction of vegetation architecture [14]. Yet this benefit comes at the expense of pricier instrumentation and the need for more sophisticated carrier platforms.

Irrespective of the chosen method, agricultural analyses most often rely on raster-centric processing chains, using canopy height models (CHM) or alternative approaches that fuse point cloud and raster representations [35-37]. A CHM portrays the upper envelope of tree crowns and their vertical offsets from the terrain; it is therefore typically derived by subtracting a digital terrain model (DTM) from a corresponding digital surface model (DSM). The necessary reference DTMs can be produced by deploying automated filtering algorithms designed to classify returns originating from the ground plane. Initially, such vegetation-filtering algorithms were conceived for LiDAR point clouds, though they may be adapted to photogrammetric contexts as well [24]. In practice, multiple software platforms implement automated vegetation filters that nonetheless continue to yield higher performance within forested landscapes than in environments dominated by low-stature plants [14, 25-27]. Fruit orchards or vineyard settings, however, are defined by isolated trees of relatively modest size, typically ranging from about 1 m up to 4 m in height [38]. An analogous situation arises with land contaminated by industrial pollutants or heavy metals that is undergoing phytoremediation or rehabilitation via the planting of woody or shrubby species capable of ameliorating the soil's chemical and physical profile and abating contaminant concentrations [39, 40]. These latter contexts are commonly marked by extremely short vegetation, on the scale of half a meter, and published examples of height retrieval applied to such settings are scarce beyond the LiDAR-focused literature. Certain potential drawbacks of the SfM workflow when applied to low-lying vegetation are explored in the contribution by Matsuura *et al.* [41], which describes a stereo-matching-based methodology for plants of relatively short stature (50–60 cm).

This contribution documents the initial outcomes of an investigation into using aerial photogrammetry collected with inexpensive UAV platforms to retrieve tree dimensional properties, specifically height. This inquiry forms part of a broader project aimed at establishing algorithms and procedural frameworks for analyzing and tracking soils burdened with heavy metals and subject to phytoremediation, grounded in the characterization of dimensional, geophysical, and biochemical parameters. The overarching aim is to develop species- and site-specific algorithms adaptable to distinct soil substrates, plant taxa, and microbial consortia, thereby enabling the identification of optimal conditions for restoring contaminated

© 2024 The Author(s). | Published by Agro Intelligence Research Press

sites. To this end, two experimental sites, designated “Area 1” and “Area 2”, possessing dissimilarities in their typical tree stature (Area 1: 5 m; Area 2: 0.70 m), were chosen to execute the geomatic surveys and to stress-test the methodology’s applicability under the taxing scenario of very young, small saplings. Three low-cost UAV sorties were flown over Area 1, each at a distinct altitude above ground to gauge the influence of image spatial resolution (ground sampling distance—GSD).

In contrast, only a single UAV flight was conducted over Area 2. Commencing with photogrammetric acquisitions, the operational pipeline entails constructing a reference digital terrain model (DTM), dense point clouds, and digital surface models (DSMs), followed by a GIS-driven routine for isolating individual tree heights using a local maxima detection algorithm. Finally, the accuracy of the extracted

Materials and Methods

Study areas

Two separate investigation sites were chosen for the analysis, distinguished by differing physical characteristics, most notably average plant height. The analytical design aimed to examine the feasibility of deploying an identical-height retrieval protocol under divergent conditions to diagnose potential constraints in the workflow. The first location, referred to as “Area 1”, constitutes a section of an olive orchard covering roughly 1.2 hectares in the southern part of Sardinia, Italy **(Figure 1a)**. Close to 80 olive trees occupy the parcel, arranged in a regimented grid along well-defined rows, with individual heights ranging from 3 m to 6 m (averaging approximately 5 m). This parcel was designated as the optimal testbed for our purposes, given its combination of moderate tree stature, crown spread, and foliage density. The second location, here termed “Area 2”, consists of nearly 600 juvenile trees arranged in 26 planting rows with a 2–3 m spacing, covering about half a hectare **(Figure 1b)**. Because the establishment of this planting formed part of a landscape rehabilitation initiative that had commenced only a handful of months before the survey campaign, plant heights in this plot are predominantly very low, ranging from 10 cm to 140 cm, and occasionally leafless. Moreover, the plantation scheme within Area 2 incorporates three distinct botanical species, each exhibiting its own characteristic foliage architecture and mature height: roughly 50 cm, 70 cm, and 85 cm for lentisk, poplar, and oleander, respectively. It warrants emphasis that this second investigation area presents exceptional difficulty due to the minimal vegetative development at the moment of the remote sensing acquisition.

© 2024 The Author(s). | Published by Agro Intelligence Research Press

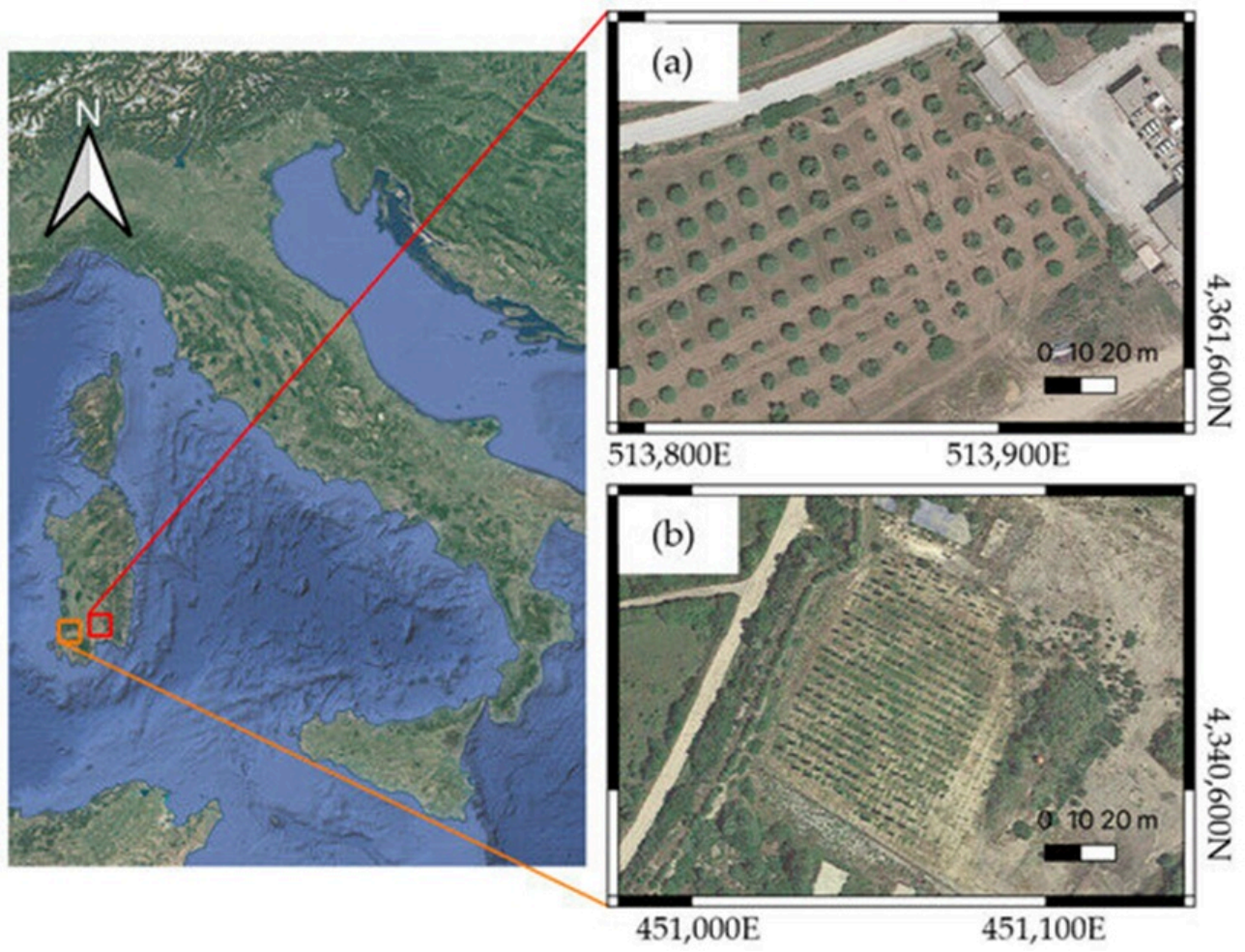

Figure 1. National- and local-scale geographic settings of the study zones in southern Sardinia, Italy: (a) pertains to Area 1 (olive orchard site), and (b) pertains to Area 2 (plantation of poplar, lentisk, and oleander). Basemap source: Google Satellite. The cartographic output was produced using QGIS software (version 3.28.15), and all coordinates are referenced to the ETRS89-ETRF2000-UTM32 datum (EPSG: 6707).

UAV photogrammetric surveys

Three UAV data acquisition campaigns were carried out in Area 1 using an exceptionally low-cost Mini 3—DJI platform fitted with an RGB camera, all flown on the same date and under identical atmospheric conditions **(Figure 2a)**. Three separate flying heights were selected, namely 50 m, 40 m, and 30 m for sorties 1, 2, and 3, respectively. The aircraft were steered manually, securing a final forward overlap of 80% and side overlap of 70%. A set of 6 GCPs was uniformly distributed, with 4 along the boundaries and 2 in the central part of the plot. A well-conceived spatial arrangement of GCPs is critical not only for robust image orientation but equally for suppressing block deformation artifacts that may arise from uncorrected systematic biases in the camera calibration [42, 43]. The GCP coordinates were captured using a single Trimble R8 GNSS receiver operating in NRTK mode for georeferencing. Northing and Easting values tied to the ETRF2000-UTM32N spatial framework (EPSG: 6707) were obtained from the Sardinian SARNET service [44]. In addition, ellipsoidal heights were converted to orthometric elevations via the ConveRgo utility [45], which taps the ITALGEO05 geoid separation grid (GK2 format) [46].

© 2024 The Author(s). | Published by Agro Intelligence Research Press



Figure 2. Planting rows and UAV flight operations across the study plots: (a) depicts Area 1, and (b) depicts Area 2, photographed while undertaking the GNSS-NRTK survey of the GCPs.

The UAV flight over Area 2, hereafter referred to as “Flight a”, was conducted with a DJI Phantom 4 quadcopter carrying RGB sensors and operating at 42 m above ground level. Here, forward and side overlaps of 80% and 70%, respectively, were ensured via an automated flight-planning module. The GCP survey adhered to the same protocol as the first plot, encompassing 7 markers uniformly distributed across the extent: 4 at the outer edges and 3 in the interior zone **(Figure 2b)**.

The GCPs were physically instantiated on the ground surface using circular red-and-white targets measuring 20 cm across at both field locations **(Figure 3)**. The form and scale of these markers were conceived to remain discernible on frames collected from altitudes reaching as high as 80 m.

© 2024 The Author(s). | Published by Agro Intelligence Research Press



Figure 3. Sample circular target utilized as a ground control point (GCP).

The key specifications of the four UAV missions are presented in **Table 1**, whereas **Table 2** catalogs the camera characteristics deployed in Areas 1 and 2.

Table 1. Consolidated overview of the UAV flight parameters for Area 1 and Area 2.

Site	Flight ID	Survey date and time	Flight altitude (m)	Flight trajectory pattern	Ground sampling distance (GSD)	Number of GCPs	Number of nadir images
Area 1	1	14 December 2023, from 11:13:49 to 11:28:22	50	North–South direction	1.61 cm/pix	6	118
Area 1	2	14 December 2023, from 11:34:23 to 11:43:51	40	North–South direction	1.14 cm/pix	6	86
Area 1	3	14 December 2023, from 11:49:56 to 11:55:42	30	North–South direction	0.53 cm/pix	6	59

© 2024 The Author(s). | Published by Agro Intelligence Research Press

Area 2	a	3 January 2023, from 10:01:22 to 10:15:22	42	Northeast–Southwest direction	1.07 cm/pix	7	345

Table 2. Camera specifications.

Site	Sensor resolution (Pixels)	Sensor pixel size (μm)	Full-frame equivalent focal length (mm)
Area 1	12 MP	2.64	24
Area 2	12.4 MP	2.41	20

UAV data processing

The gathered imagery was processed within the Agisoft Metashape environment, version 2.0.4 [47]. Metashape is a proprietary software solution extensively embraced across academic circles and by geomatics practitioners for the production of orthophotomosaics, digital elevation products, and volumetric reconstructions. The platform operationalizes the structure-from-motion (SfM) paradigm, together with multi-view stereo (MVS) algorithms. The SfM algorithm delivers fully autonomous image orientation and a low-density scene model. The exterior orientation parameters of the images, the three-dimensional locations of matched features, and the intrinsic camera calibration terms were globally refined through bundle block adjustment [48-50]. Beyond this, Metashape adopts a hierarchical scheme for SfM reconstruction known as HSfM, which can be viewed as a direct evolution of incremental SfM (ISfM) [51]. MVS procedures were subsequently invoked to derive the dense point cloud and to assemble the 3D surface models that underpin the DSMs and orthophotos [38, 52].

For each UAV dataset, we followed the standard processing sequence prescribed by the software, comprising the following steps: image loading, image matching and alignment, sparse cloud construction, camera alignment optimization, dense cloud reconstruction, and spatial referencing. A total of 118, 86, 59, and 345 near-vertical frames were recorded for Flights 1, 2, 3, and Flight “a”, respectively **(Table 1)**, and every image contributed successfully to the alignment phase. The dense clouds were built using the high-quality preset, which, in Metashape, triggers an initial downsampling of the source imagery by a factor of 4, or halving along each image dimension.

The dense reconstructions were tied to the ground reference system through 6 GCPs for the Area 1 blocks and 7 GCPs for the Area 2 block. The standard deviation (SD) along with the lower and upper extremes of the georeferencing residuals are listed in **Table 3**.

Table 3. Standard deviation (SD), minimum, and maximum figures for the georeferencing residual errors. Quantities are stated in centimetres.

Site	Flight ID	Number of GCPs	Minimum–maximum accuracy in Z (cm)	Minimum–maximum accuracy in Y (cm)	Minimum–maximum accuracy in X (cm)	Standard deviation (cm) (X; Y; Z)
Area 1	1	6	−3.3; 2.9	0.3; 5.4	−1.2; 2.4	1.4; 2.8; 2.3
Area 1	2	6	−8.5; 1.6	−3.8; 2.8	−0.4; 1.6	0.9; 2.5; 6.5
Area 1	3	6	−3.0; 11.3	−3.0; 13.3	−9.5; 2.8	6.1; 7.9; 7.2

© 2024 The Author(s). | Published by Agro Intelligence Research Press

Area 2	a	7	−1.7; 2.2	−1.3; 1.1	−1.8; 4.0	1.8; 0.8; 2.2

As **Table 3** shows, the inflated SD figures for Flight 3 over Area 1 are conspicuous, and the underlying causes were explored. Even though scrutinizing the multiple GCPs across the images and their collimation did not yield a clear explanation, the decision was made to retain this dataset and examine how it behaves within the intended processing chain.

Table 4 enumerates the point population within each cloud, along with the corresponding disk storage footprint; the dense cloud originating from Flight 1 is shown in **Figure 4** as an illustrative example.



© 2024 The Author(s). | Published by Agro Intelligence Research Press

Figure 4. Dense point cloud produced from Flight 1 (Area 1).

Table 4. Point cloud properties are expressed through point population and file footprint.

Site	Flight	N points	File size
Area 1	1	82 million	2.30 GB
	2	104 million	2.52 GB
	3	95 million	2.31 GB
Area 2	a	105 million	2.55 GB

For every UAV sortie, the dense point clouds were spatially interpolated in the CloudCompare software suite (version 2.12.14) [53], yielding the respective DSM with a grid cell size of 20 cm. The methodology subsequently adopted sought to isolate tree heights by capitalizing on a pre-existing digital terrain model of the locality, obtained through an external channel, and by applying UAV-derived data to synthesize the reference DTM. Adopting this tactic was also made viable by the virtually flat topographic gradient characterizing both chosen experimental plots. While it is true that CHMs result from a normalization of surface heights, subdued terrain inclines enable independent DTM processing without incurring meaningful distortions arising from the interpolation stage [10]. That being said, mindful of the divergent natures of the two case studies with respect to plant stature and crown spread, marginally dissimilar filtering strategies were pursued to derive the reference DTM. To elaborate, Area 1 hosts fully grown olive trees with well-separated crowns, whereas Area 2 harbors at least small shrub-like vegetation. As a result, the routine automated classification operations—that is, the embedded classification algorithms supplied by the Agisoft Metashape and CloudCompare platforms—proved inapplicable to the second site. Over Area 1, the automated filter implemented within CloudCompare (Cloth Simulation Filter—CSF) was applied to partition the UAV dense cloud into “terrain” and “above-terrain” subsets. The chosen CSF parameterization was as follows: cloth resolution 1.0; iteration ceiling 1000; and classification cutoff 0.5. Vegetation stripping for the second dataset was instead performed interactively, harnessing the open-source LAStool toolkit [54] integrated into the QGIS platform [55]. A clipping operation was performed on the dense cloud, excising crown returns from the native point set. Following the classification step, the DTMs for both sites were generated by interpolating the terrain-classified points using the Rasterize module in CloudCompare, with a grid cell size of 20 cm.

GIS-based approach for tree height extraction

The raster layers representing height variation were derived as the arithmetic difference between each DSM and its partner DTM, making use of the Raster Calculator utility inside QGIS software:

$$\mathrm{CHM} = \mathrm{DSM} - \mathrm{DTM}, \quad (1)$$

Where the output map corresponds to the canopy height model (CHM) [33].

In the final stage, the CHM raster products were interrogated within the GIS workspace via a local maxima detection strategy. Concretely, the CHM cell values within the polygon envelopes delineating individual trees were identified using the Zonal Statistics tool in QGIS. This function computes various summary statistics for raster pixels within user-defined zones. Following the logic of the local maxima approach, the peak pixel values retrieved are the strongest candidates for coinciding with tree apex locations. They are thereby designated as the UAV-inferred tree heights. Owing to the highly regimented row layouts characteristic of both Area 1 and Area 2, no redundant detections of tree summits were encountered, a complication that can arise in more structurally intricate vegetation communities [56]. On these grounds, the maximum values were isolated and assigned to each tree for the downstream analysis. **Figure 5** supplies a schematic depiction of the full processing pipeline leading to tree height recovery.

© 2024 The Author(s). | Published by Agro Intelligence Research Press

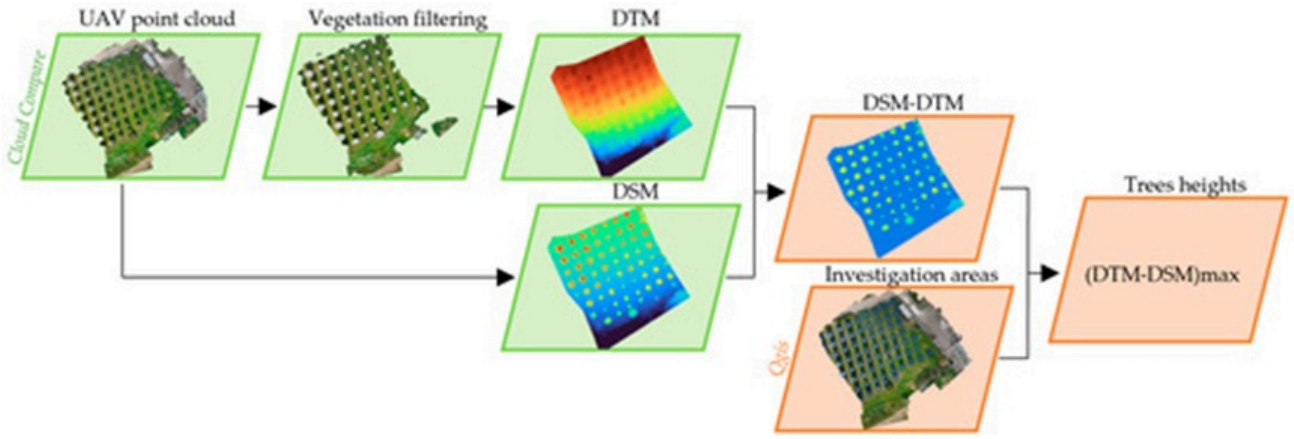

Figure 5. Flowchart summarizing the operational sequence for tree height extraction.

Field measurements of tree heights and statistical analysis

Every UAV flight mission was paired with concurrent ground-truth observations destined for the accuracy assessment protocol. To be precise, the stature of each plant was directly gauged using a graduated measuring staff. The field-recorded values were linked to the mapped tree positions using a GIS-based procedure, generating an exhaustive site inventory that specifies planting row, unique identification code, botanical species (relevant for Area 2), and plant height. These records are henceforth referred to as “field measurements”.

The fidelity of the tree height determination was evaluated using a range of statistical indices. Residuals (r), capturing the offset between each i-th UAV-retrieved height and its counterpart field-surveyed value, were examined, as formalized in **Eq. 2**.

$$r_i = h_{est,i} - h_{meas,i}, \quad (2)$$

Where h_{est} and h_{meas} denote the UAV-estimated stature and the in-situ measured stature, respectively, the smallest, largest, mean, and standard deviation (SD) of the residual distribution were computed for each flight, along with the 50% and 90% percentiles. Beyond this, to portray the connection between the observed errors and the associated plant sizes, the average relative error ($\underline{r}\%$) was determined per flight, following **Eq. 3**.

$$\underline{r}\% = \frac{\sum_{i=1}^{n} r_i / h_{meas,i}}{n} \cdot 100, \quad (3)$$

With n standing for the tally of trees.

Ultimately, the overall departure between the field-surveyed values and the extracted tree heights was quantified by the root mean square error (RMSE), as specified in **Eq. 4**.

$$RMSE = \sqrt{\frac{\sum_{i=1}^{n} (h_{est,i} - h_{meas,i})^2}{n}}, \quad (4)$$

© 2024 The Author(s). | Published by Agro Intelligence Research Press

The outcomes are presented visually as frequency distributions of residuals, and the association between the extracted and measured heights is shown in scatter plots overlaid with linear regression fits. The R^2 statistics from each linear regression serve as quantitative metrics for assessing accuracy. In addition, box-and-whisker diagrams were constructed to convey a graphical sense of the dispersion characterizing both the estimated and the directly measured tree heights.

Results and Discussion

The core statistical summaries of the residual differences between the extracted and in situ-measured heights, organized by flight, are presented in **Table 5**.

Table 5. Residuals between estimated tree heights and field-surveyed values: minimum, maximum, and mean figures, standard deviations, together with the 50th and 90th percentile thresholds, are supplied for each flight. All quantities are stated in metres.

Site	Flight	90%ile (m)	50%ile (m)	SD (m)	Mean (m)	Max (m)	Min (m)
Area 1	1	0.72	0.38	0.34	−0.34	0.70	−1.13
	2	0.87	0.31	0.44	−0.26	1.37	−1.30
	3	0.49	0.16	0.28	0.14	1.46	−0.42
Area 2	a	0.96	0.57	0.24	−0.62	−0.04	−1.37

Focusing on Area 1, the outcomes fall within the accuracy range anticipated for taller trees or forestry-related applications, with absolute mean residual values ranging from 14 cm to 34 cm. As would be predicted, lower flight altitude —that is, a finer GSD—yields progressively closer correspondence with the ground-reference observations, following the sequence from Flight 1 to Flight 3. In particular, Flight 3 (at an altitude of 30 m) shows very encouraging results, with fully 90% of the residuals remaining below 50 cm. This outcome also came as a partial surprise, given the elevated RMSE values observed during the georeferencing stage **(Table 3)**. A distinction among the three sorties is nevertheless apparent, since the first two generally tend to under-predict tree stature.

In contrast, the third leans towards a modest over-prediction (treating the field measurements as the reference in the differencing, as formalized in **Eq. 2**). This behaviour is equally evident in the residual frequency distribution histograms shown in **Figure 6a** and should be further explored to identify potential causal factors. Although Flight 3 covered a somewhat reduced footprint relative to the previous acquisitions, with a sum of 41 trees identified, a near-Gaussian spread of the differences, centered not far from zero, can still be observed. To conclude the analysis, the connection between the residuals and the matching “true” height (sourced from the field survey) was probed through the r% indicator. Markedly similar values emerge for Flights 1 and 2, standing at 8.7% and 8.8%, respectively, whereas for Flight 3 the r% equals 5.5%. These outcomes affirm the satisfactory performance at the first site, indicating that the errors—understood as the residuals of the height estimation—are small relative to the absolute tree sizes. This conclusion is further supported by the RMSE values of 0.47 m, 0.51 m, and 0.37 m for Flights 1, 2, and 3, respectively.

© 2024 The Author(s). | Published by Agro Intelligence Research Press

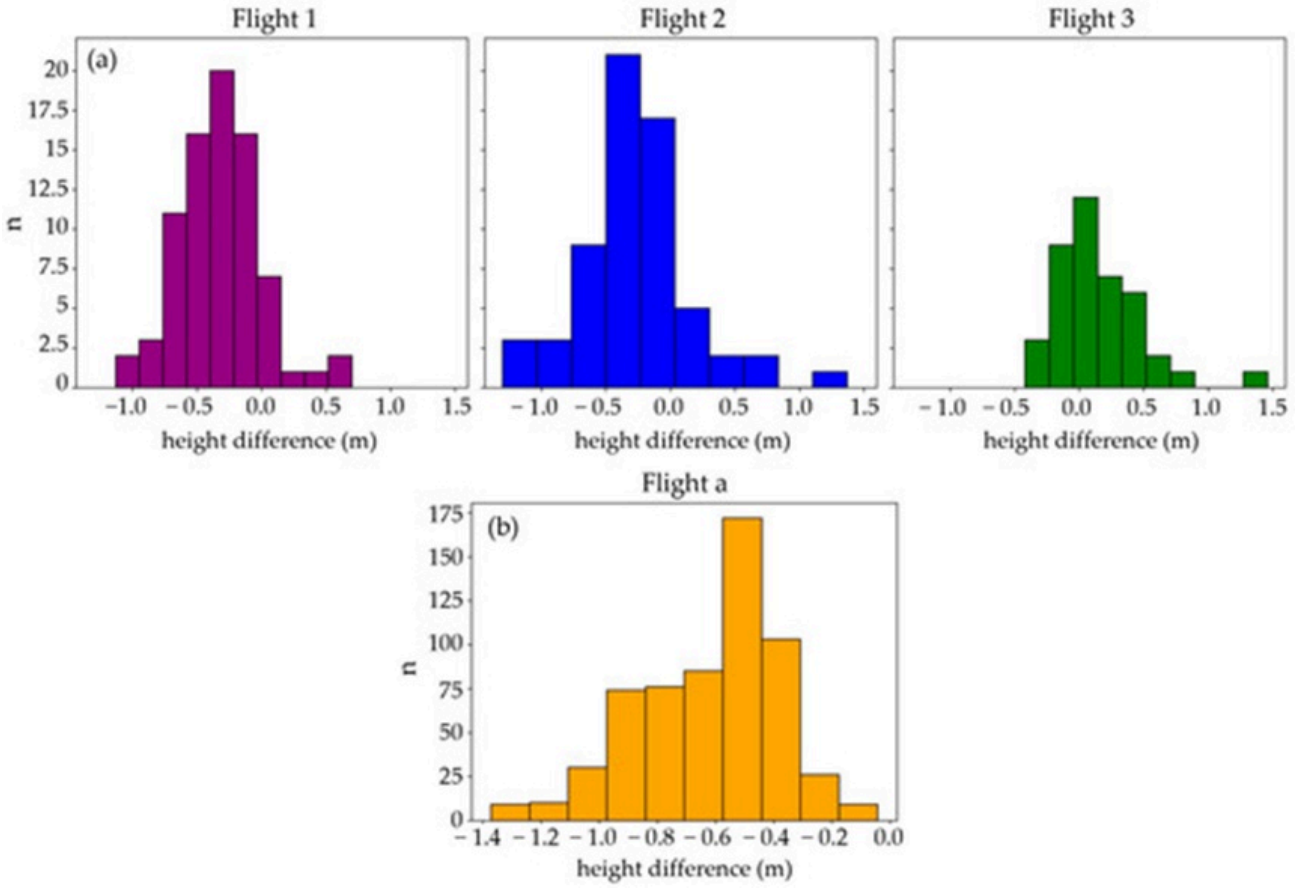

Figure 6. Frequency distribution histograms of the residuals between the extracted and field-measured tree heights: (a) Area 1—Flights 1, 2, and 3, and (b) Area 2—Flight a.

A sharply contrasting picture emerges in Area 2, where **Table 5** and **Figure 6b** show that the residuals are uniformly shifted toward negative values, with a mean of approximately -60 cm, about 30 cm larger in absolute terms than the poorest-performing flight in Area 1 (Flight 1). Such a finding was anticipated from a cursory visual appraisal of the dense point cloud, in which the vegetation was only faintly perceptible, largely because of its extremely modest stature. This limitation propagated throughout the processing chain. As an initial consideration, independent of any subsequent processing, it proved troublesome to obtain a faithful depiction of very young saplings within the dense photogrammetric cloud, given their constrained crown dimensions and sparse foliage. In the second place, low vegetation heights adversely affect the filtering stage, which cannot be automated and instead requires manual intervention. As a concluding point, comparing DSMs and DTMs—both products of interpolation procedures that introduce their own uncertainty contributions—demands sufficient accuracy for small-amplitude variations to be reliably detected. It stands to reason that these elements exert a reciprocal influence on one another, alongside the plant heights themselves, which are simultaneously the source of the difficulty and the reason the technique proves inapplicable within this setting. Indeed, even if the field measurements are recognized to carry uncertainties below the centimetre level, the disparities obtained approach, and at times exceed, the actual tree heights encountered across the plot. Furthermore, the RMSE value also supports the conclusion, with a value of 0.67 m.

Figure 7 displays the box-and-whisker plots contrasting the estimated and directly measured tree heights for the three sorties over Area 1. The minimum, maximum, and median figures for both data series are highlighted, revealing the greater dispersion of the estimated quantities relative to the measured ones, as well as the tendency toward under-prediction for the first two sorties, a trend that reverses in the case of Flight 3. It bears noting that, given the residual-

© 2024 The Author(s). | Published by Agro Intelligence Research Press

based statistics had already laid bare the behaviour in Area 2, a deliberate decision was made to forgo presenting box charts for the second experimental site.

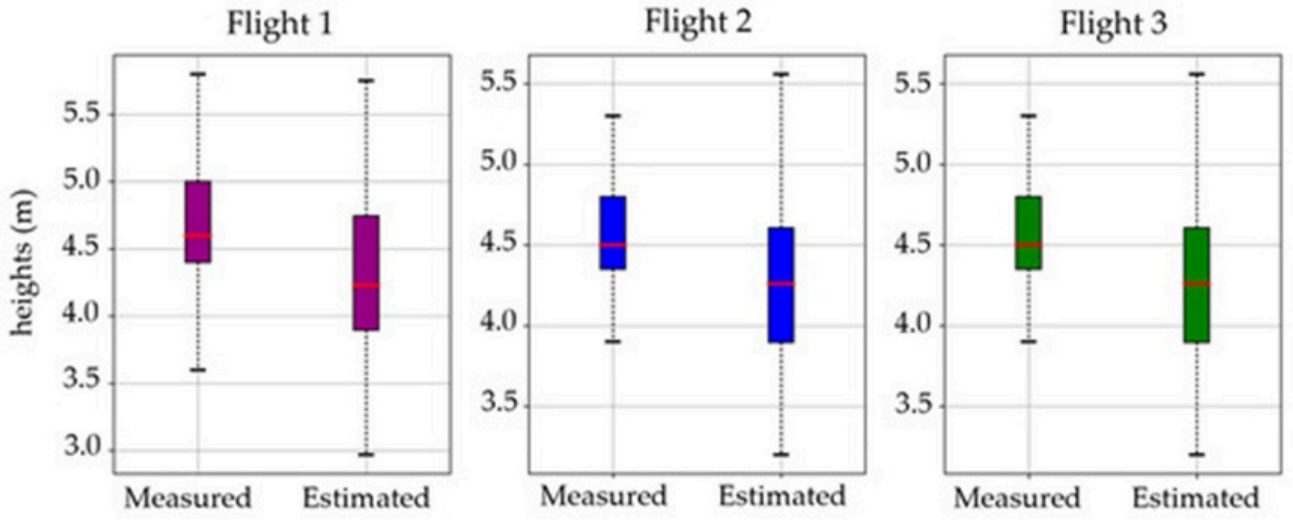

Figure 7. Box-and-whisker plots showing the variance in measured and estimated tree heights across the three sorties in Area 1.

The linkage between the estimated and the field-measured tree heights across the three sorties conducted in Area 1 is set out in **Figure 8**. Examination of the superimposed linear regression lines suggests that, overall, the models—i.e., the collection of estimated height values—reproduce the field-observed samples. Flight 1 and Flight 3 display broadly similar coefficients of determination (R^2 = 0.67; R^2 = 0.65), whereas the figure is somewhat reduced for Flight 2 (R^2 = 0.50). Remarks similar to those expressed for the earlier plots apply to the Area 2 dataset depicted in **Figure 8**.

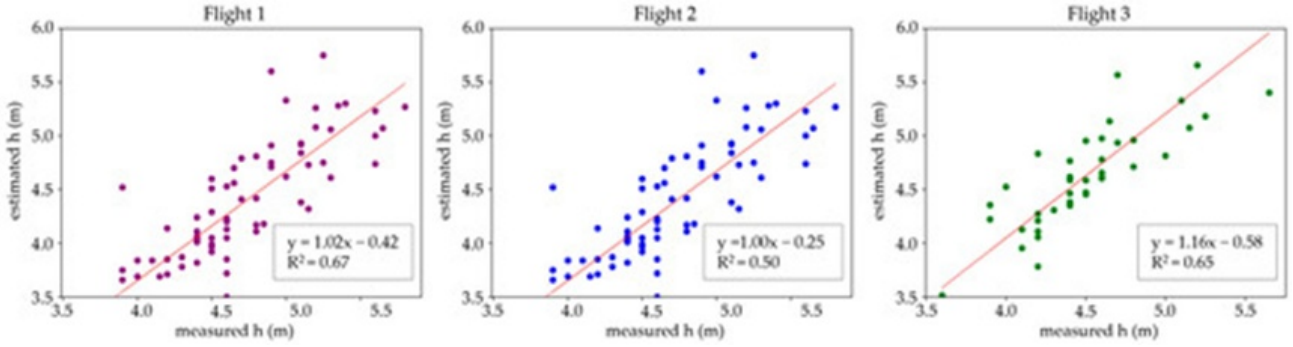

Figure 8. Relationship between estimated and field-measured tree heights, ordinary least-squares regression lines, and associated parameters for the three UAV campaigns over Area 1.

Presently, the observation and management of agricultural landscapes are of considerable importance in environmental safeguarding and precision agriculture (PA), driven in part by the European Common Agricultural Policy (CAP) [57, 58]. A steadily expanding body of associated research is indeed emerging, within which geomatic survey methodologies occupy a pivotal role.

This work centers on exploiting photogrammetric datasets to recover dimensional descriptors of trees. Initial findings on tree height estimation from imagery collected with low-cost UAV platforms are presented. The advocated methodology is anchored in photogrammetric processing that capitalizes on SfM, coupled with a GIS-mediated analytical phase. This analytical stage remains uncomplicated and relies predominantly on open-source software packages, specifically

© 2024 The Author(s). | Published by Agro Intelligence Research Press

CloudCompare and QGIS, again rendering the entire pipeline highly adaptable. Two trial sites, referred to as “Area 1” and “Area 2”, were selected, and a combined set of four UAV acquisitions was flown. From UAV dense point clouds, reference DTMs were generated either by automated filtering routines or by manual classification of ground and vegetation returns. The canopy height models, constructed by subtracting each DTM from its corresponding DSM, were interrogated in the GIS workspace using a local maxima detection algorithm, with purpose-drawn zones serving as individual examination neighborhoods around each tree. In this fashion, the candidate tree summits, matching the peak CHM pixel values, were located, and the heights read at those positions were carried forward into the subsequent analysis. The availability of concurrent in-field measurements alongside the UAV collections underpinned the validation phase and the statistical examination, enabling a quantitative appraisal of the methodology’s fidelity.

Within Area 1, the comparison with field-surveyed data yielded encouraging results, with absolute mean residuals ranging from 14 to 34 cm. The most favorable figures are associated with the sortie flown at 30 m above ground, substantiating the notion that image spatial resolution (GSD) is a critical parameter for achieving superior quality in photogrammetric deliverables. This conclusion likewise finds backing in other studies, for instance, Kameyama and Sugiura [22] and Pourreza *et al.* [29]. In particular, Pourreza *et al.* [29] deployed a DJI Phantom 4 at a series of altitudes (25 m, 50 m, and 100 m) over a site whose tree statures are analogous to those examined here, corroborating that accuracy exhibits an inverse dependence on flight elevation. Furthermore, all sorties over Area 1 display 50% of their residuals falling below 38 cm, and the residual frequency distribution histograms assume near-Gaussian forms. Outcomes at the first site also align with those reported in a comparable investigation by Zarco-Tejada *et al.* [28], who obtained an RMSE of 35 cm for trees with heights ranging from 1.16 m to 4.38 m.

Regarding the determination coefficients for height retrieval, their higher value ($R^2 = 0.83$ vs. our $R^2 = 0.67$) could stem from differences in the ground-truth observations used for validation. We are conscious, indeed, that the employment of a graduated measuring pole is unavoidably susceptible to meteorological factors, notably wind, to the inherent characteristics of the trees with respect to foliage density and crown geometry, and to the subjective element that colors the readings. Birdal *et al.* [26] reported an RMSE of 28 cm for trees ranging from 1.2 m to 7.1 m, which aligns well with our results, whereas their R^2 statistic is notably higher (0.95). Analogous findings appear in Wallace *et al.* [14], Krause *et al.* [21], Yurtseven *et al.* [23], and Gülci [31], whose documented RMSE and R^2 values are consistent with ours in contexts featuring taller vegetation. Even so, the results from the separate sorties over the first site reveal divergent tendencies, since Flights 1 and 2 broadly under-predict the trees’ statures, while Flight 3 tends toward over-prediction. Given that the literature generally supports the presence of an underestimation bias in UAV-extracted heights [21, 29], this phenomenon warrants further inquiry, which will be the subject of future investigations.

As was to be expected, the circumstances encountered in Area 2 prompted starkly different conclusions, seeing that the average residual hovers near −60 cm—that is, at times greater in absolute terms than the actual tree heights encountered across the plot. Even though the flight altitude remained broadly comparable to that of Flight 1, the average residual was 30 cm larger. This situation can reasonably be ascribed not solely to the altitude but rather to the “absolute” size of the individual trees, which rendered the entire workflow exceedingly challenging. We wish to underline once more the complexity of the deliberately chosen scenario for Area 2, where tree heights are uniformly below 1.5 m, and the foliage is only modestly developed. Three principal factors were pinpointed as shaping this outcome: (i) the degree to which the photogrammetric dense cloud faithfully captures very short saplings; (ii) the necessity for manual vegetation removal; and (iii) the influence of interpolation during the generation and subsequent differencing of the DSM and DTM. Although the results obtained render the technique unworkable for this range of heights, we sought, given the presence of multiple plant species across Area 2, to draw some connection between the outputs and species identity. No clear signal has emerged, barring a marginally more favorable response from lentisk relative to the other two taxa (poplar, oleander); however, it seems plausible that dependable species-level discrimination would require taller individuals to permit differentiation based on foliage architecture and crown reach.

Considered in their entirety, the obtained findings substantiate the suitability of UAV photogrammetric data captured using inexpensive instrumentation for tree height retrieval. Transferring the same analytical pipeline to multi-temporal datasets

© 2024 The Author(s). | Published by Agro Intelligence Research Press

collected at low flight altitudes could also enable the estimation of tree growth increments over medium- to long-term temporal horizons. Such data are pivotal for examining phytoremediation processes when assessing plant vitality and the effectiveness of the selected remediation strategy. Furthermore, because low-cost UAV equipment remains readily accessible to non-specialist operators, the possibility of adopting an identical workflow is a tangible benefit for all those active in the agricultural domain. That said, applying the same methodology in settings dominated by very short tree saplings calls for additional inquiry, and conceivable near-term advances of this research might include UAV sorties flown at even lower altitudes, alongside an intermediate case study revisiting Area 2 once the vegetation has undergone a phase of growth.

Conclusion

Finally, it is worth emphasizing that this investigation sits within the framework of a larger-scale project, “Tecnologie di CARatterizzazione Monitoraggio e Analisi per il ripristino e la bonifica (CARMA)”, which involves the integration of both geomatics and geophysical data [59]. Thus, the study presented here represents a first move toward attaining the project’s objectives of merging geometric, biochemical, and geophysical information into a unified analytical protocol for assessing tree health and growth rhythms. With this multidisciplinary horizon in mind, future developments may include the deployment of more sophisticated technologies, such as LiDAR, to enhance accuracy, particularly across zones occupied by very short saplings. In addition, forthcoming analyses will draw upon both nadir and oblique frames, as advocated in Birdal *et al.* [26] and Pourreza *et al.* [29]. Indeed, incorporating oblique imagery improves final accuracy by enabling the reconstructed point cloud to better register the ground surface beneath and immediately adjacent to trees, yielding superior classification outcomes.

Acknowledgements

The authors are grateful to Pasquale Carta, Andrea Dessì, Sergio De Montis, and Federico Secchi for their contributions during the field surveys.

Conflict of interest

None

Financial support

This research was funded by Sardegna Ricerca, CUP: G28C17000250006, https://www.ecoserdiana.com/servizi/progetti-di-ricerca.html (accessed on 5 January 2024).

Ethics statement

None

Received: 07 Dec 2022 Revised: 11 Feb 2023 Accepted: 28 Feb 2023
Published online: 25 May 2024

Rights and permissions

© 2024 The Author(s). | Published by Agro Intelligence Research Press

Open Access The author(s) retain copyright. This article is licensed under the Creative Commons Attribution-NonCommercial-ShareAlike 4.0 International License. It may be shared and adapted for non-commercial purposes with appropriate attribution, an indication of changes, and distribution of adaptations under the same license. Third-party material may be subject to separate terms identified in its credit line. View the license at https://creativecommons.org/licenses/by-nc-sa/4.0/.

References

1. Ammoniaci M, Kartsiotis SP, Perria R, Storchi P. State of the art of monitoring technologies and data processing for precision viticulture. Agriculture. 2021;11:201.

2. Pagliai A, Ammoniaci M, Sarri D, Lisci R, Perria R, Vieri M, et al. Comparison of aerial and ground 3D point clouds for canopy size assessment in precision viticulture. Remote Sens. 2022;14:1145.

3. Crookston RK. A top 10 list of developments and issue impacting crop management and ecology during the past 50 years. Crop Sci. 2006;46:2253-62.

4. Casa R, Airoldi G, Balsari P, Basso B, Boschetti M, Buttafuoco G, et al. Agricoltura diprecisione. Metodi etecnologie per migliorare l'efficienza e lasostenibilità dei sistemi colturali. In: Agricoltura di Precisione; Edagricole—Edizioni Agricole di New Business Media srl: Milano, Italy, 2016. https://www.edagricole.it/wp-content/uploads/2020/03/5510-Agricoltura-di-precisione-SFOGLIA.pdf (accessed on 1 September 2023).

5. Vacca G, Quaquero E. BIM-3D GIS: An integrated system for the knowledge process of the buildings. J Spat Sci. 2020;65:193-208.

6. Belcore E, Angeli S, Colucci E, Musci MA, Aicardi I. Precision agriculture workflow, from data collection to data management using FOSS tools: An application in Northern Italy vineyard. ISPRS Int J Geo-Inf. 2021;10:236.

7. Hobart M, Pflanz M, Weltzien C, Schirrmann M. Growth height determination of tree walls for precise monitoring in apple fruit production using UAV photogrammetry. Remote Sens. 2020;12:1656.

8. Zaru N, Rossi M, Vacca G, Vignoli G. Spreading of localized information across an entire 3D electrical resistivity volume via constrained EMI inversion based on a realistic prior distribution. Remote Sens. 2022;15:3993.

9. Gonzalez-Dugo V, Zarco-Tejada P, Nicolás E, Nortes PA, Alarcón JJ, Intrigliolo DS, et al. Using high-resolution UAV thermal imagery to assess the variability in the water status of five fruit tree species within a commercial orchard. Precis Agric. 2013;14:660-78.

10. Vecchi E, Tavasci L, De Nigris N, Gandolfi S. GNSS and photogrammetric UAV derived data for coastal monitoring: A case of study in Emilia-Romagna, Italy. J Mar Sci Eng. 2021;9:1194.

11. Zhang HL, Tian WT, Yin J. A review of unmanned aerial vehicle low-altitude remote sensing (UAV-LARS) use in agricultural monitoring in China. Remote Sens. 2021;13:1221.

12. Remondino F, Barazzetti L, Nex F, Scaioni M, Sarazzi D. UAV photogrammetry for mapping and 3D modelling–current status and future perspectives. Int Arch Photogramm Remote Sens Spat Inf Sci. 2012;38:25-31.

13. Wallace L. Assessing the stability of canopy maps produced from UAV-LiDAR data. In Proceedings of the IEEE International Geoscience and Remote Sensing Symposium-IGARSS, Melbourne, Australia; 2013. p. 3879–82.

14. Wallace L, Lucieer A, Malenovský Z, Turner D, Vopěnka P. Assessment of forest structure using two UAV techniques: A comparison of airborne laser scanning and structure from motion (SfM) point clouds. Forests. 2016;7:62.

15. Argamosa RJL, Paringit EC, Quinton KR, Tandoc FAM, Faelga RAG, Ibañez CAG, et al. Fully automated GIS-based individual tree crown delineation based on curvature values from a lidar derived canopy height model in a coniferous plantation. Int Arch

Photogramm Remote Sens Spat Inf Sci. 2016;41:563-9.

16. Beloiu M, Heinzmann L, Rehush N, Gessler A, Griess VC. Individual tree-crown detection and species identification in heterogeneous forests using aerial RGB imagery and deep learning. Remote Sens. 2023;15:1463.

17. Tiede D, Hochleitner G, Blaschke T. A full GIS-based workflow for tree identification and tree crown delineation using laser scanning. In: Proceedings of the ISPRS Workshop CMRT 2005, Vienna, Australia; August 2005;5.

18. Latella M, Sola F, Camporeale C. A density-based algorithm for the detection of individual trees from LiDAR data. Remote Sens. 2021;13:322.

19. Velusamy P, Rajendran S, Mahendran RK, Naseer S, Shafiq M, Choi JG. Unmanned aerial vehicles (UAV) in precision agriculture: Applications and challenges. Energies. 2022;15:217.

20. Panagiotidis D, Abdollahnejad A, Slavik M. 3D point cloud fusion from UAV and TLS to assess temperate managed forest structures. Int J Appl Earth Obs Geoinf. 2022;112:102917.

21. Krause S, Sanders TG, Mund JP, Greve K. UAV-based photogrammetric tree height measurement for intensive forest monitoring. Remote Sens. 2019;11:758.

22. Kameyama S, Sugiura K. Estimating tree height and volume using unmanned aerial vehicle photography and SfM technology, with verification of result accuracy. Drones. 2020;4:19.

23. Yurtseven H, Akgul M, Coban S, Gulci S. Determination and accuracy analysis of individual tree crown parameters using UAV based imagery and OBIA techniques. Measurement. 2019;145:651-64.

24. Komárek J, Klápště P, Hrach K, Klouček T. The potential of widespread UAV cameras in the identification of conifers and the delineation of their crowns. Forests. 2022;13:710.

25. Huo L, Lindberg E, Holmgren J. Towards low vegetation identification: A new method for tree crown segmentation from LiDAR data based on a symmetrical structure detection algorithm (SSD). Remote Sens Environ. 2022;270:112857.

26. Birdal AC, Avdan U, Türk T. Estimating tree heights with images from an unmanned aerial vehicle. Geomat Nat Hazards Risk. 2017;8:1144-56.

27. Moudrý V, Klápště P, Fogl M, Gdulová K, Barták V, Urban R. Assessment of LiDAR ground filtering algorithms for determining ground surface of non-natural terrain overgrown with forest and steppe vegetation. Measurement. 2020;150:107047.

28. Zarco-Tejada PJ, Diaz-Varela R, Angileri V, Loudjani P. Tree height quantification using very high resolution imagery acquired from an unmanned aerial vehicle (UAV) and automatic 3D photo-reconstruction methods. Eur J Agron. 2014;55:89-99.

29. Pourreza M, Moradi F, Khosravi M, Deljouei A, Vanderhoof MK. GCPs-free photogrammetry for estimating tree height and crown diameter in Arizona Cypress plantation using UAV-mounted GNSS RTK. Forests. 2022;13:1905.

30. Surový P, Ribeiro NA, Panagiotidis D. Estimation of positions and heights from UAV-sensed imagery in tree plantations in agrosilvopastoral systems. Int J Remote Sens. 2018;39:4786-800.

31. Gülci S. The determination of some stand parameters using SfM-based spatial 3D point cloud in forestry studies: An analysis of data production in pure coniferous young forest stands. Environ Monit Assess. 2019;191:495.

32. Lisein J, Pierrot-Deseilligny M, Bonnet S, Lejeune P. A photogrammetric workflow for the creation of a forest canopy height model from small unmanned aerial system imagery. Forests. 2013;4:922-44.

33. Mohan M, Silva CA, Klauberg C, Jat P, Catts G, Cardil A, et al. Individual tree detection from unmanned aerial vehicle (UAV) derived canopy height model in an open canopy mixed conifer forest. Forests. 2017;8:340.

© 2024 The Author(s). | Published by Agro Intelligence Research Press

34. Pearse GD, Dash JP, Persson HJ, Watt MS. Comparison of high-density LiDAR and satellite photogrammetry for forest inventory. ISPRS J Photogramm Remote Sens. 2018;142:257-67.

35. Belcore E, Latella M. Riparian ecosystems mapping at fine scale: A density approach based on multi-temporal UAV photogrammetric point clouds. Remote Sens Ecol Conserv. 2022;8:644-55.

36. Dandois JP, Ellis EC. High spatial resolution three-dimensional mapping of vegetation spectral dynamics using computer vision. Remote Sens Environ. 2013;136:259-76.

37. Popescu SC. Estimating biomass of individual pine trees using airborne lidar. Biomass Bioenergy. 2007;31:646-55.

38. Vacca G. Estimating tree height using low-cost UAV. Int Arch Photogramm Remote Sens Spatial Inf Sci. 2023;48:381-6.

39. Naveed M, Ghaffar M, Khan Z, Gul N, Ijaz I, Bibi A, et al. Morphological and structural responses of Albizia lebbeck to different lead and nickel stress levels. Agriculture. 2023;13:1302.

40. Wang Y, Wang S, Zhao Z, Zhang K, Tian C, Mai W. Progress of Euhalophyte adaptation to arid areas to remediate salinized soil. Agriculture. 2023;13:704.

41. Matsuura Y, Heming Z, Nakao K, Qiong C, Firmansyah I, Kawai S, et al. High-precision plant height measurement by drone with RTK-GNSS and single camera for real-time processing. Sci Rep. 2023;13:6329.

42. Shahbazi M, Sohn G, Théau J, Menard P. Development and evaluation of a UAV-photogrammetry system for precise 3D environmental modeling. Sensors. 2015;15:27493-524.

43. Sanz-Ablanedo E, Chandler JH, Rodríguez-Pérez JR, Ordóñez C. Accuracy of unmanned aerial vehicle (UAV) and SfM photogrammetry survey as a function of the number and location of ground control points used. Remote Sens. 2018;10:1606.

44. Sarnet, Web Server della Rete di Stazioni Permanenti Della Sardegna. www.sarnet.it/servizi.html (accessed on 1 January 2024).

45. Centro Interregionale per I Sistemi Informatici Geografici e Statistici In Liquidazione. Trasformazioni di Coordinate—Il Software ConveRgo. https://www.cisis.it/?page_id=3214 (accessed on 1 January 2024).

46. International Service for the Geoid (ISG). Italy (ITALGEO05). https://www.isgeoid.polimi.it/Geoid/Europe/Italy/italgeo05_g.html (accessed on 1 January 2024).

47. AgiSoft PhotoScan Standard (Version 1.2.6) (Software). 2016. http://www.agisoft.com/downloads/installer/ (accessed on 27 January 2024).

48. Turner D, Lucieer A, Watson C. An automated technique for generating georectified mosaics from ultra-high resolution unmanned aerial vehicle (UAV) imagery, based on structure from motion (SfM) point clouds. Remote Sens. 2012;4:1392-410.

49. Szeliski R. Computer vision: Algorithms and applications; Springer Nature: Berlin/Heidelberg, Germany, 2022.

50. Jiang S, Jiang C, Jiang W. Efficient structure from motion for large-scale UAV images: A review and a comparison of SfM tools. ISPRS J Photogramm Remote Sens. 2020;167:230-51.

51. Liang Y, Yang Y, Fan X, Cui T. Efficient and accurate hierarchical SfM based on adaptive track selection for large-scale oblique images. Remote Sens. 2023;15:1374.

52. Lingua AM, Maschio P, Spadaro A, Vezza P, Negro G. Iterative refraction-correction method on Mvs-Sfm for shallow stream bathymetry. Int Arch Photogramm Remote Sens Spat Inf Sci. 2023;XLVIII-1/W1-2023:249-55.

© 2024 The Author(s). | Published by Agro Intelligence Research Press

53. CloudCompare. https://www.danielgm.net/cc/ (accessed on 1 January 2024).

54. Isenburg, M. LAStools—Efficient LiDAR Processing Software (Version 141017, Unlicensed). http://rapidlasso.com/LAStools (accessed on 1 September 2023).

55. QGIS Documentation. https://docs.qgis.org/2.8/en/ (accessed on 1 January 2024).

56. Panagiotidis D, Abdollahnejad A, Surový P, Chiteculo V. Determining tree height and crown diameter from high-resolution UAV imagery. Int J Remote Sens. 2017;38:2392-410.

57. European Commission. Agriculture and Rural Development, Common Agricultural Policy. https://agriculture.ec.europa.eu/common-agricultural-policy_en#:~:text=The%20CAP%20is%20a%20partnership,27%20commenced%201%20January%202023 (accessed on 1 January 2024).

58. Alexandratos N, Bruinsma J. World agriculture towards 2030/2050: The 2012 revision; ESA Working Paper 2012 12-03; FAO: Rome, Italy, 2012.

59. Ecoserdiana. Progetto di Ricerca su Tecnologie di CARatterizzazione Monitoraggio e Analisi per il Ripristino e la Bonifica (CARMA)—Fondo Europeo di Sviluppo Regionale—Por Fesr Sardegna 2014–2020. https://www.ecoserdiana.com/servizi/progetti-di-ricerca.html (accessed on 1 December 2023).

© 2024 The Author(s). | Published by Agro Intelligence Research Press